Journal of Hazardous Materials 381 (2020) 120908

Contents lists available at ScienceDirect

Journal of Hazardous Materials

journal homepage: www.elsevier.com/locate/jhazmat

Evaluation of single and combined toxicity of bisphenol A and its analogues using a highly-sensitive micro-biosensor

Xiaolin Zhu[a], Guanlan Wu[a], Yi Xing[a], Chengzhi Wang[a], Xing Yuan[a,*], Baikun Li[b,**]

[a] School of Environment, Northeast Normal University, Changchun 130117, PR China
[b] Department of Civil & Environmental Engineering, University of Connecticut, Storrs, CT 06269, USA

GRAPHICAL ABSTRACT

A micro-biosensor based on the screen printed electrode (SPE) modified with carboxylated multi-walled carbon nanotube/rhodamine B/gold nanoparticles (MWCNTs-COOH/RhB/AuNPs) was developed to evaluate the single and combined toxicity of BPA and its analogues on Ctenopharyngodon idella kidney (CIK) cells.

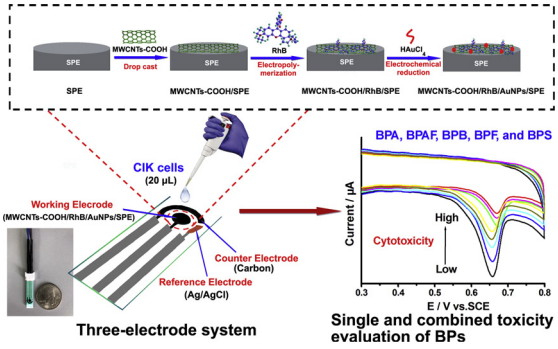

ARTICLE INFO

Editor: A. Daugulis

Keywords:
Bisphenol analogues
CIK cells
Combined toxicity
Screen printed electrode
Micro-biosensor

ABSTRACT

Bisphenol analogues have been developed as alternatives to bisphenol A (BPA), a common chemical with potential adverse effects on human health. It is imperative to perform a fast and sensitive evaluation for the toxicity of these bisphenol analogues. This study introduces a label-free electrochemical biosensor based on a screen-printed electrode modified with the carboxylated multi-walled carbon nanotube/rhodamine B/gold nanoparticle. Ctenopharyngodon idella kidney (CIK) cells were used as the biological recognition agent to detect changes in electrochemical signals and indicate the cell viability. Only 20 μL of sample was required for detection, which was much lower than that of other conventional electrochemical methods (≥ 1 mL). This biosensor was examined for the cytotoxicity of BPA, bisphenol AF (BPAF), bisphenol B (BPB), bisphenol F (BPF), and bisphenol S (BPS) to CIK cells. The half inhibition concentration (IC_{50}) values after 48 h of exposure indicated that the rank order of cytotoxicities was BPAF > BPB > BPA > BPF > BPS. The morphological changes in CIK cells after treatment with various bisphenols were investigated, and the combined toxicities of the binary bisphenol mixtures were determined. Potentially synergistic and additive effects were observed. These findings provide new insights into the cytotoxicity of bisphenol analogues.

* Corresponding author at: School of Environment, Northeast Normal University, Changchun 130117, PR China.
** Corresponding author at: Department of Civil & Environmental Engineering, University of Connecticut, Storrs, CT 06269, USA.
E-mail addresses: yuanx@nenu.edu.cn (X. Yuan), baikun.li@uconn.edu (B. Li).

https://doi.org/10.1016/j.jhazmat.2019.120908
Received 16 April 2019; Received in revised form 10 July 2019; Accepted 17 July 2019
Available online 18 July 2019

1. Introduction

As the polymerization agent for epoxy resin and polycarbonate, bisphenol A (BPA) is an endocrine disruptor and raises the increased concerns over its safety (Kitamura et al., 2005; Kwak et al., 2018; Villeneuve et al., 2011; Hou et al., 2017). The use of BPA-based coating in infant formula packaging has been prohibited in the United States of America (U.S. Food and Drug Administration, 2013). Accordingly, other bisphenols referred to as BPA-related compounds or bisphenol analogues that consist of two phenolic rings joined together via a carbon bridge or another structure, have been utilized in the manufacture of resins and plastics in recent years (Liao and Kannan, 2014). These bisphenols have been normally disposed in aquatic environments, where the health impacts are documented for numerous aquatic organisms. Bisphenols have been found in the rivers in China, Japan, and India, even at concentrations higher than BPA (Jin and Zhu, 2016; Liu et al., 2017; Yamazaki et al., 2015). Due to their similar chemical structures and binding affinities for the estrogen receptor, bisphenols are likely to have similar physiological effects on organisms (Mu et al., 2018; Qiu et al., 2018; Zhu et al., 2018a). However, compared with the numerous reports on BPA, studies on the cytotoxicity of bisphenols, as well as the combined toxicity with BPA, are still limited. The safety of bisphenols is currently debated and their toxic effects have not yet been established. Therefore, a more sensitive and comprehensive evaluation of their toxicity is urgently needed.

Novel electrochemical biosensor based on the nucleotide metabolism of cells has received extensive attention on account of its simplicity, high sensitivity, low cost, and real-time measurement (Zhu et al., 2018b). Compared with conventional methyl-thiazolyl-tetrazolium (MTT) cell viability assays, the electrochemical cell-based biosensor is rapid and label-free without the need of color developing agents, and directly detects intracellular purine bases (Zhu et al., 2016, 2014). It is a reliable tool for the cytotoxicity screening of anticancer drugs, environmental estrogens, and heavy metals (Guo et al., 2015; Zhu et al., 2017; Wu et al., 2011). Several cancer cells, including human cervical carcinoma HeLa cells, human breast cancer MCF-7 cells, and human hepatoma HepG2 cells, have been used to establish models. However, normal (non-cancerous) cells have rarely been studied. Additionally, due to the large size of the conventional glassy carbon electrodes (GCEs), a high number of cells are needed. It is critical to develop miniaturized and low-cost electrodes with high sensitivity.

Screen printed electrodes (SPE), which have several advantages over conventional electrodes, have received high attention (Johari-Ahar et al., 2018; Salgado-Figueroa et al., 2015). The advantages of large-scale production, cost-effectiveness, disposability, and feasibility make SPE a favorable candidate for on-the-spot and real-time detection (Li et al., 2012). SPE is constructed from commercial conductive carbon ink and is commonly used as the substrate electrode. However, its poor electrochemical activity has limited its application. Thus, other nanomaterials such as carbon nanotubes, grapheme, and nanoparticles, have been used to modify the SPE surface to improve its electrochemical performance (Ochiai et al., 2017; Jirasirichote et al., 2017; Charoenkitamorn et al., 2018).

Gold nanoparticles (AuNPs) have attracted considerable attention due to their large surface area, excellent catalytic ability, fast electron transfer rate, enhanced electrical conductivity, and surpassing ability to immobilize biomolecules (Hassani et al., 2018). AuNPs have been applied in the detection of various analytes, such as insulin, BPA, and chloramphenicol (Wang et al., 2015; Li et al., 2016; Bagheri Hashkavayi et al., 2015). The size, shape, and structure of AuNPs are directly related with their electrochemical properties (Saxena and Goswami, 2012). Therefore, the matrix used to prepare highly dispersed AuNPs is important. Multi-walled carbon nanotubes (MWCNTs) are good carrier materials with low electrical resistance, high electrical conductivity, and excellent mechanical strength (Wang, 2005). Furthermore, the combined use of AuNPs and MWCNTs can produce synergistic effects on their electrocatalytic properties. Compared with conventional chemical and thermal methods, the electrochemical reduction method has the advantages of being rapid and cost-effective, and can prepare composites by reducing Au^{3+} rapidly under cathodic conditions (Alim et al., 2018; Magar et al., 2017; Yue et al., 2015). As an oxadiazole organic dye, rhodamine B (RhB) can increase the potential window, surface area, and stability of the modified electrode (Thomas et al., 2012). Electropolymerization of RhB is primarily carried out by tertiary amine cations, and positive charges may be preferred for binding to negatively charged surfaces (Zhu et al., 2018c). Functionalized MWCNTs can be negatively charged due to the presence of −COOH, C−OH, and C−O−C groups. Thus, RhB can be used to non-covalently modify functionalized MWCNTs to form the polymeric film with high performance.

Herein, we developed a facile approach to synthesize MWCNTs-COOH/RhB/AuNPs to enhance the sensitivity and selectivity of SPE. The amount of cells required was reduced to one-fiftieth of the conventional amount. The sensitive and stable Ctenopharyngodon idella kidney (CIK) cells were used as the ideal substrate for toxicity testing (Tan et al., 2008, 2014). There were three objectives in this study. First, MWCNTs/RhB/AuNPs/SPE was developed and characterized. Second, the electrochemical behavior of CIK cells was investigated. Third, the micro-biosensor was used in evaluating the single and combined toxicity of BPA and its analogues, including bisphenol S (BPS), bisphenol AF (BPAF), bisphenol B (BPB), and bisphenol F (BPF) (Fig. 1).

2. Experimental

2.1. Reagents and solutions

Carboxylated multi-walled carbon nanotubes (MWCNTs-COOH, purity > 95%, diameter 30–50 nm, length 0.5–2.0 μm) were purchased

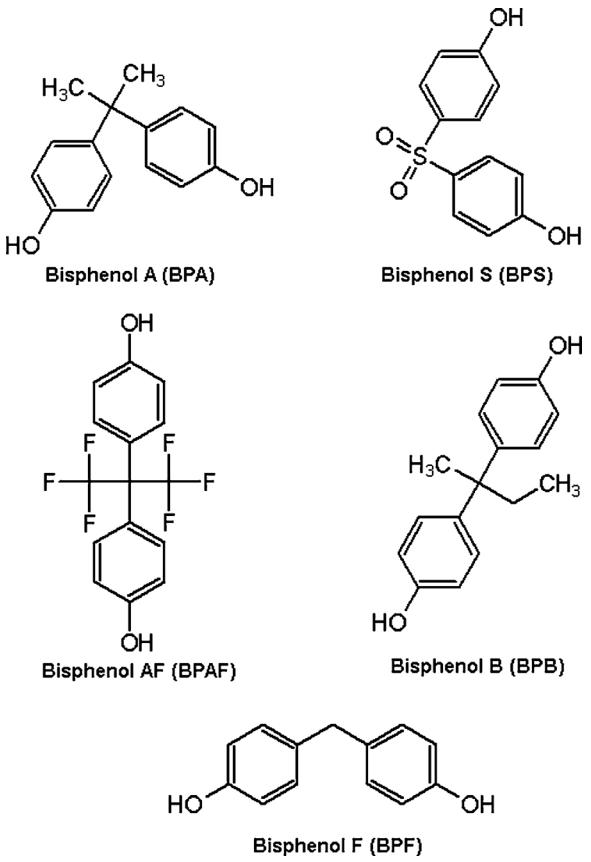

Fig. 1. Chemical structures of the five bisphenols tested in this study.

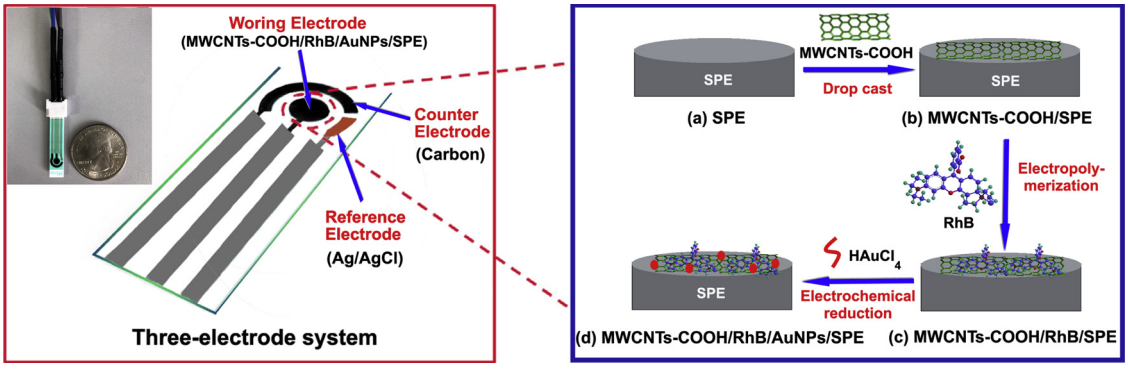

Fig. 2. Fabrication of the MWCNTs-COOH/RhB/AuNPs/SPE.

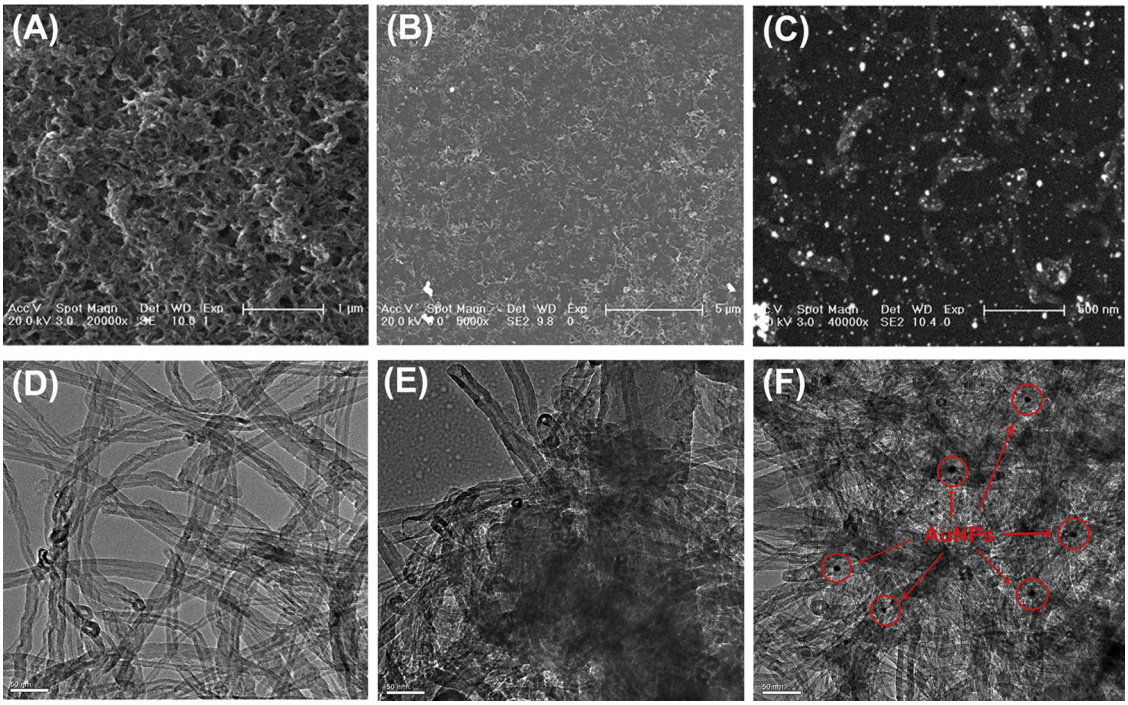

Fig. 3. SEM images of MWCNTs-COOH (A), MWCNTs-COOH/RhB (B), and the MWCNTs-COOH/RhB/AuNPs composite (C); TEM images of MWCNTs-COOH (D), MWCNTs-COOH/RhB (E), and the MWCNTs-COOH/RhB/AuNPs composite (F).

from XFNANO Materials TECH Co., Ltd. (Nanjing, China). A screen-printed carbon electrode (SPE) was purchased from Mxense Bio-Tech Co., Ltd. (Ningbo, China). Sulfuric acid (H_2SO_4), hydrochloric acid (HCl), N-methyl pyrrolidone (NMP), and other analytical reagents were purchased from J & K. Trypsin was purchased from Sigma (St. Louis, MO, USA). BPA, BPAF, BPB, BPF, BPS, RhB, and gold chloride trihydrate ($HAuCl_4{\cdot}H_2O$) were obtained from Aladdin Reagent Co., Ltd. (Shanghai, China). Phosphate buffered saline (PBS, 0.1 M Na_2HPO_4 and 0.1 M KH_2PO_4, pH 7.4) was prepared. All other chemicals were of analytical grade and used as received.

2.2. Apparatus

All electrochemical measurements were performed with a CHI 760E electrochemical workstation (Shanghai CH Instruments, China). The SPE was used as the disposable all-solid-state sensor. The carbon was insulated, with the exposure of a diameter of 2.5 mm for the working electrode. Pure carbon was used as the counter electrode, and Ag/AgCl was used as the reference electrode. Scanning electron microscopy (SEM) images were obtained with a XL-30 ESEM electron microscope (FEI Co.). Transmission electron microscopy (TEM) images were recorded in a JEM-2010 high resolution transmission electron microscope (Japan). Energy dispersive X-ray spectroscopy (EDS) was carried out with an Oxford Instrument. Raman spectra were recorded with a confocal microprobe Raman system (HR 800, Jobin Yvon) using a 488 nm Ar^+ laser. The morphologies of CIK cells were recorded by an inverted microscope (BDS-400, Chongqing Optec Instrument Co., China). The pH was measured with a pH meter (Sartorius PB-10, Germany).

2.3. Cell culture

CIK cells (Shanghai BioLeaf Biotech Co., Ltd, China) were cultured in minimum essential medium (Corning, NY, USA) supplemented with 10% fetal bovine serum (Gibco, USA), 1% penicillin (100 U mL^{-1}), and streptomycin (100 μg mL^{-1}) at 28 °C in 5% CO_2 in a humidified atmosphere.

2.4. Preparation of MWCNTs-COOH/RhB/AuNPs/SPE

Ten milligrams of MWCNTs-COOH was dispersed in 10.0 mL of NMP and sonicated for 3 h. Three microliters of the mixed solution was

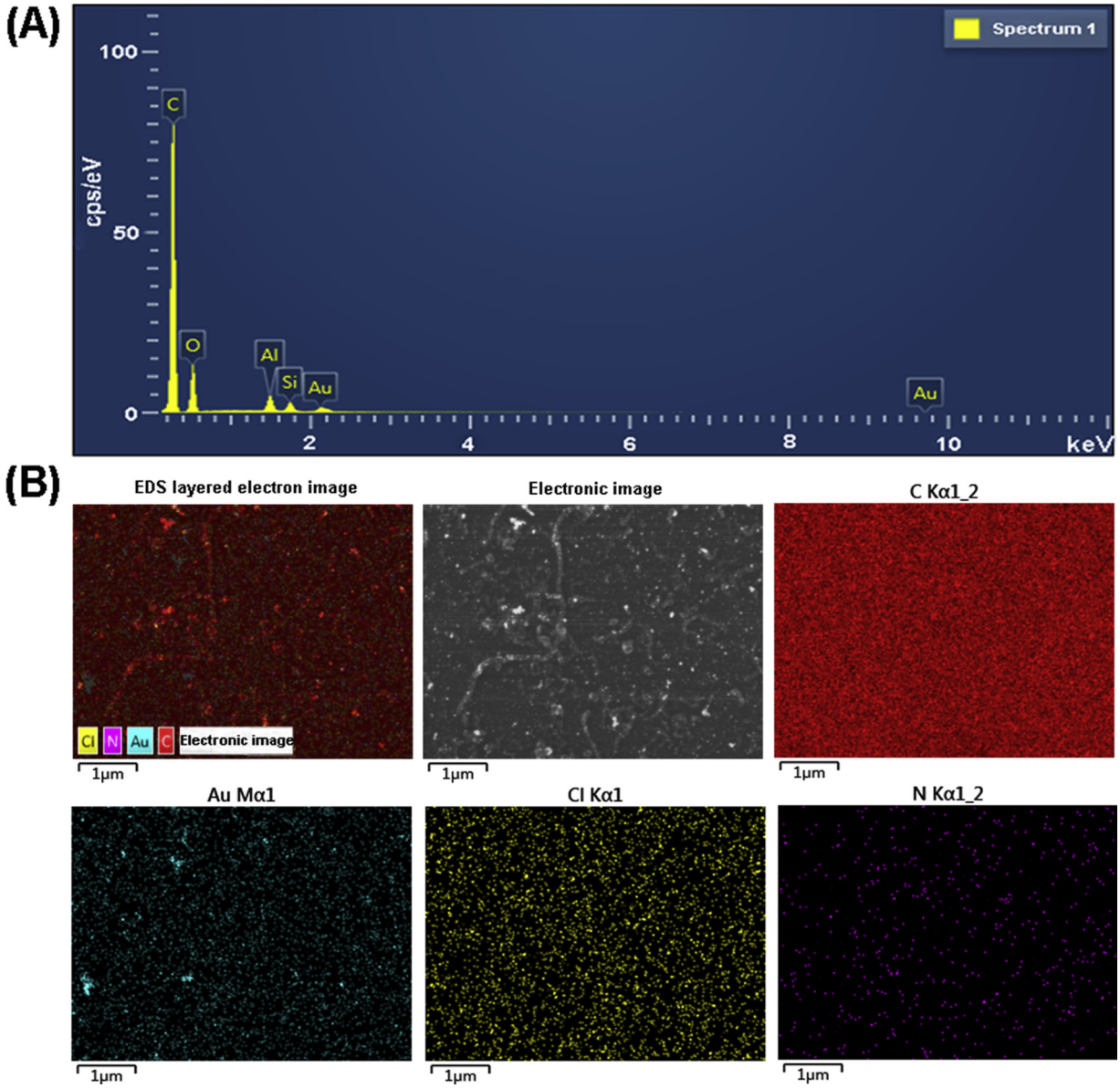

Fig. 4. Typical EDS spectrum (A) and EDS layered mapping (B) of the MWCNTs-COOH/RhB/AuNPs/ITO.

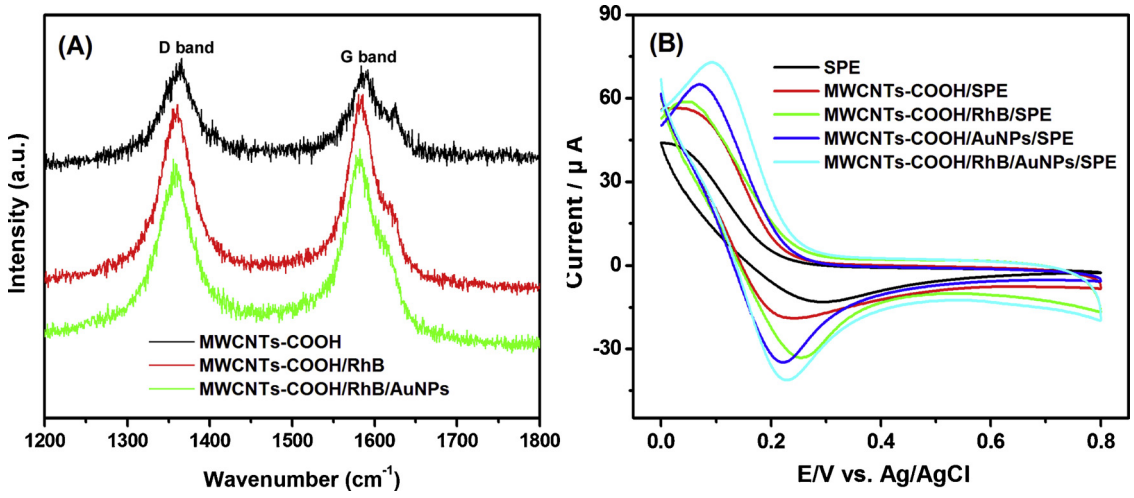

Fig. 5. (A) Raman spectra of MWCNTs-COOH, MWCNTs-COOH/RhB, and the MWCNTs-COOH/RhB/AuNPs composite; (B) Cyclic voltammograms of 5.0 mM $K_3[Fe(CN)_6]$ solution containing 0.1 M KCl at different electrodes with the scan rate of 50 mV s^{-1}.

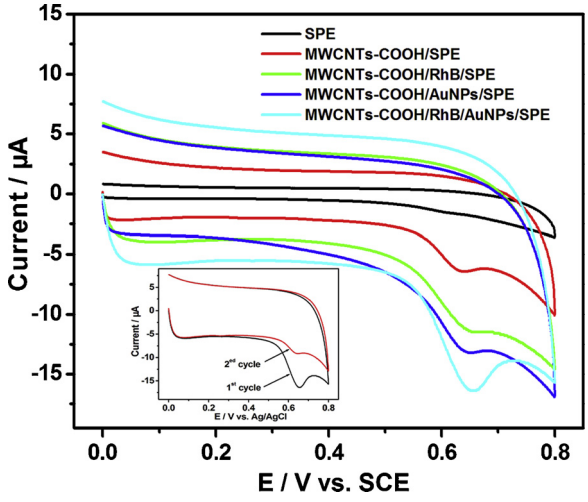

Fig. 6. Cyclic voltammograms of CIK cells on SPE, MWCNTs-COOH/SPE, MWCNTs-COOH/RhB/SPE, MWCNTs-COOH/AuNPs/SPE, and MWCNTs-COOH/RhB/AuNPs/SPE. Inset: Cyclic voltammograms of CIK cells on MWCNTs-COOH/RhB/AuNPs/SPE at the first and second scan. Cell concentration: 1.0×10^6 cells mL^{-1}.

dropped onto the SPE working electrode and dried. The RhB film was electrochemically deposited in 0.1 M PBS pH 7.0 containing 25 μM RhB and 0.3 mM KNO_3 by applying the potential from -1.3 V to +1.1 V with a scan rate of 100 mV s^{-1} for ten cycles. The MWCNTs-COOH/RhB/SPE was immersed in the solution containing 1.0 mM $HAuCl_4$, 0.01 M Na_2SO_4, and 0.01 M H_2SO_4, and repetitively scanned for three cycles between +1.5 V and -0.5 V by cyclic voltammetry. The MWCNTs-COOH/RhB/AuNPs/SPE was rinsed with distilled water. The general protocol for the fabrication of the electrochemical sensor is illustrated in Fig. 2.

2.5. Single and combined cytotoxicity evaluation of bisphenols

The growth medium was replaced with the fresh medium containing BPAF, BPB, BPA, BPF, or BPS at concentrations of 2.1, 4.7, 10.3, 22.3, 48.6, 105.6, 230.0, or 500.0 μM, respectively. The same culture conditions were provided for both the control and experimental groups. After 48 h of cultivation, the medium was aspirated and sterile PBS was added. The CIK cell suspension was prepared by heating the solution in a water bath set at 50 °C for 30 min (Wu et al., 2011). One drop (~20 μL) of the cell suspension was dropped onto the SPE for the electrochemical determination. The accumulation process was carried out using amperometric detection with the following parameters: init E, 0 V; sample interval, 0.05 s; quite time, 1 s; and run time, 360 s. Cyclic voltammetry was performed in the range of 0 ± 0.8 V with a scan rate of 50 mV s^{-1}. The cytotoxicity was calculated using the following formula:

$$\text{Cytotoxicity} = (I_{p,1} - I_{p,2})/I_{p,1} \times 100\%,$$

where $I_{p,1}$ and $I_{p,2}$ are the peak currents of the control and experimental groups, respectively.

The combined toxicity evaluation was based on the toxic unit (TU) concept ($TU = C/IC_{50}$, where C is the toxicant exposure concentration in the mixture) (Broderius et al., 1995). The total TU of the mixture was obtained by summing the ratios of the concentrations of each bisphenol in the mixture and then dividing by its IC_{50} when present alone. The combined effect is described as follows: if a mixture having a sum $TU = 1 \pm 0.2$ caused 50% growth inhibition, the combined toxicity is simply additive (concentration addition), whereas $TU < 0.8$ indicates potential synergism (more than additive) and $TU > 1.2$ represents potential antagonism (less than additive). The concentrations of the binary mixtures were diluted on the equitoxic basis to obtain five concentrations (sum TU at 0.2, 0.4, 0.8, 1.6, and 3.2).

2.6. Statistical analyses

All data analyses were performed with SPSS 19.0 (SPSS Inc., USA) and Origin 8.0. Each data point represents a mean of three independent sample replicates with error bars indicating the standard deviation. One-way ANOVA was used to analyze the values. P-values < 0.05 were considered significant.

3. Results and discussion

3.1. Characterization of MWCNTs-COOH/RhB/AuNPs/SPE

The morphologies of MWCNTs-COOH, MWCNTs-COOH/RhB and MWCNTs-COOH/RhB/AuNPs were observed using SEM and TEM. MWCNTs-COOH exhibited self-assembly and tubular structures (Fig. 3 A and Fig. 3 D), which are characteristic of carbon nanotubes (Subramanian et al., 2016). After the electrochemical deposition of RhB, a thin and homogeneous film was observed on MWCNTs-COOH/RhB (Fig. 3 B and Fig. 3 E), suggesting that RhB was effectively combined with MWCNTs-COOH via π-π conjugation. For MWCNTs-COOH/RhB/AuNPs (Fig. 3 C and Fig. 3 F), the AuNPs were uniformly attached to MWCNTs-COOH/RhB, indicating that the electrochemical reduction method can be used to prepare AuNPs with good dispersibility. The above results demonstrated that the composite was successfully prepared by electrochemical methods. The AuNPs could promote the electron transfer of the MWCNTs-COOH/RhB/AuNPs complex. Additionally, the composite was highly conjugated and exhibited a larger specific surface area, thus enhancing the capture of the intracellular molecules.

The chemical composition of MWCNTs-COOH/RhB/AuNPs was analyzed using EDS (Fig. 4). The bright spots distributed on MWCNTs-COOH were AuNPs. The composite was mainly composed of C, O, N, Al, and Au. Si was derived from the ITO conductive glass substrate.

Raman spectroscopy is a powerful method for characterization of the carbon structure. The D band at ~1350 cm^{-1} was caused by the disorder induced phonon mode of the sp^3 carbon atoms vibrations, which represented defects and disordered structures. The G band at ~1580 cm^{-1} corresponded to the zone center mode, specifically to the ordered sp^2-bonded carbon atoms (Zanganeh et al., 2014). The ratio of the intensity of the D band to that of the G band (I_D/I_G) represented the degree of disorder and the average size of the sp^2 domains (Dinh et al., 2015). The crystallinities and structures of MWCNTs-COOH, MWCNTs-COOH/RhB, and MWCNTs-COOH/RhB/AuNPs were studied using the Raman spectroscopy (Fig. 5 A). MWCNTs-COOH showed prominent peaks at 1362 cm^{-1} (D band) and 1589 cm^{-1} (G band). MWCNTs-COOH/RhB exhibited the D band at 1358 cm^{-1} and G band at 1583 cm^{-1}, and corresponding peaks for MWCNTs-COOH/RhB/AuNPs were observed at 1357 cm^{-1} and 1581 cm^{-1}. The D band shifted to a smaller wave number, indicating a higher level of disorder and a greater number of defects during the synthesis of the composite. Compared with MWCNTs-COOH, the I_D/I_G value of the composite decreased, which was caused by the successful introduction of RhB and AuNPs into the carbon network of MWCNTs-COOH.

The cyclic voltammogram of different electrodes in $[Fe(CN)_6]^{3-/4-}$ was used to analyzed the surface status and the barriers to electron transfer (Fig. 5 B) (Lin et al., 2014). The peak potential separation (ΔE_p) at the bare SPE was ~237 mV, indicating a relatively slow electron transfer. The MWCNTs-COOH/SPE exhibited a pair of distinct current peaks with a ΔE_p of 175 mV, indicating that the presence of MWCNTs-COOH accelerated the electron transfer kinetics as a result of the excellent conductivity and large specific surface area. The peak current at MWCNTs-COOH/RhB/SPE further increased with a ΔE_p of 189 mV, implying that the electropolymerization of RhB enhanced the electron transfer process. The peak current was enhanced with a ΔE_p of 166 mV

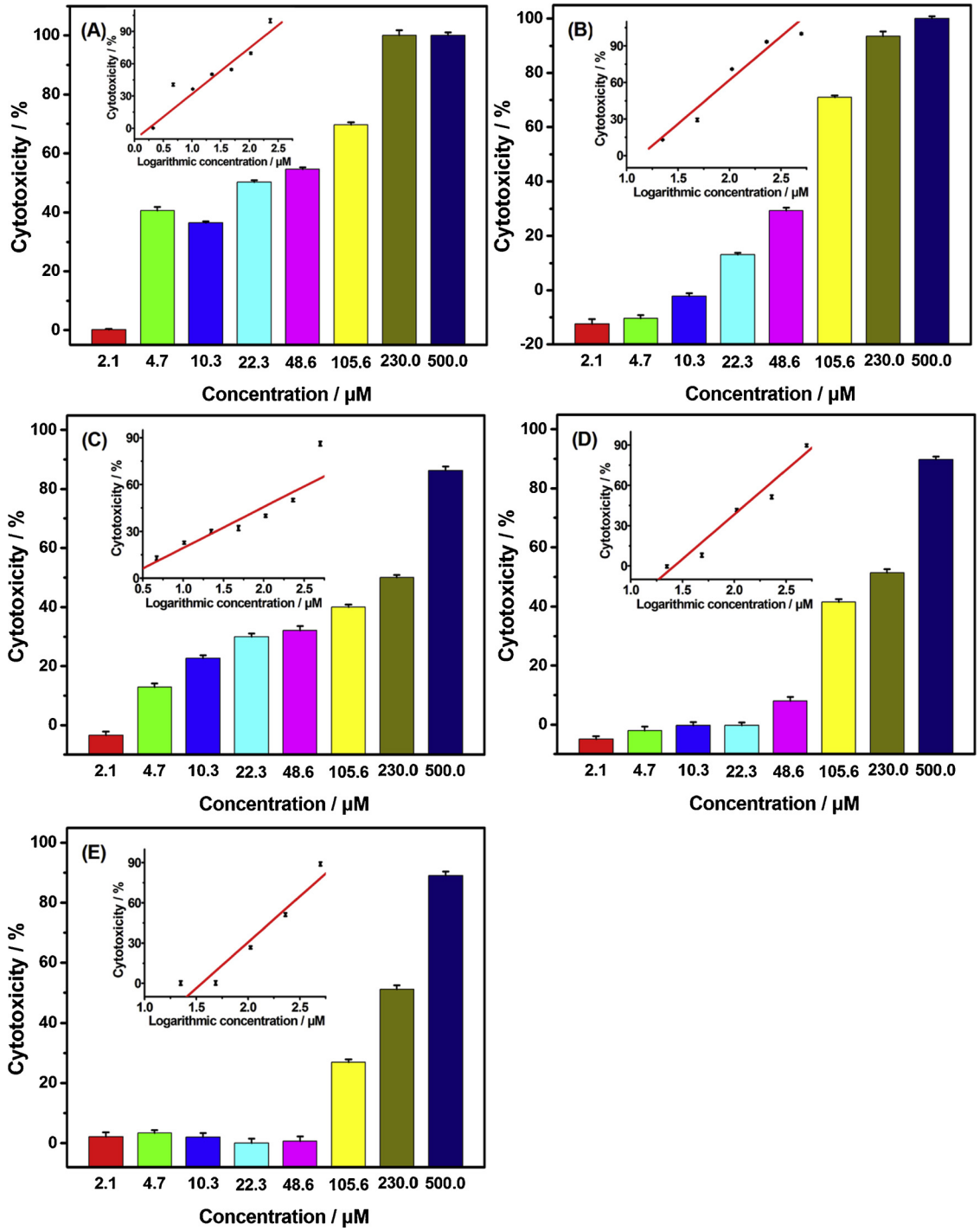

Fig. 7. Cytotoxicity of BPAF (A), BPB (B), BPA (C), BPF (D), and BPS (E) on CIK cells detected by the micro-biosensor. Inset: linear regression curve of the logarithmic concentration of the bisphenol and its cytotoxicity on CIK cells.

at MWCNTs-COOH/AuNPs/SPE, which was attributed to the good electrical conductivity and large surface-to-volume ratio of AuNPs. The best peak shape with the smallest ΔE_p of 142 mV was observed at MWCNTs-COOH/RhB/AuNPs/SPE, demonstrating that the composite greatly facilitated the reversible redox reaction.

The electrochemically active surface area (A) of electrodes can be calculated using the following formula (Guo et al., 2011):

$$I_p = (2.99 \times 10^5) n A C D^{1/2} v^{1/2},$$

where n, C, D, and v are the number of electrons in the redox process, the reactant concentration of $Fe(CN)_6^{3-/4-}$, the diffusion coefficient ($6.30 \times 10^6\ cm^2\ s^{-1}$), and the scan rate, respectively. The electroactive surface areas were calculated as 0.033 cm^2, 0.042 cm^2, 0.053 cm^2, 0.061 cm^2, and 0.073 cm^2 for SPE, MWCNTs-COOH/GCE, MWCNTs-COOH/RhB/GCE, MWCNTs-COOH/AuNPs/SPE, and MWCNTs-COOH/RhB/AuNPs/SPE, respectively, which revealed a synergistic effect among MWCNTs-COOH, AuNPs, and RhB.

3.2. Voltammetric behavior of CIK cells

The cyclic voltammetric behaviors of CIK cells on different electrodes revealed that there were no peak on the bare SPE (Fig. 6, curve

Table 1
Linear equations and correlation coefficients between the concentration and cytotoxicity of the five bisphenols on CIK cells.

Toxicant	Equation	r	IC_{50} (μM)
BPAF	$Y = 39.61\ X - 3.10$	0.921	21.33
BPB	$Y = 70.51\ X - 81.35$	0.948	72.44
BPA	$Y = 30.77\ X - 13.11$	0.905	112.20
BPF	$Y = 66.18\ X - 95.85$	0.953	158.49
BPS	$Y = 66.55\ X - 99.04$	0.963	173.78

X represents the logarithm of the concentration of bisphenols and *Y* represents the cytotoxicity (percent inhibition).

Table 2
Combined toxicities of the binary mixtures of bisphenols on CIK cells.

	Binary mixturesa	IC_{50} (sum TU)[a]	Mixture effects[b]
Group 1	BPAF + BPA	0.84	Additive
Group 2	BPB + BPA	1.15	Additive
Group 3	BPF + BPA	0.72	Synergistic
Group 4	BPS + BPA	0.76	Synergistic

[a] TU = toxicity unit.
[b] Mixture effects definition (Broderius et al., 1995): IC_{50} (TU) < 0.8 = synergistic; $0.8 \leqq IC_{50}$ (TU) $\leqq 1.2$ = simple additive; IC_{50} (TU) > 1.2 = antagonistic.

a). An oxidation peak with a peak current of 3.8 μA appeared at +0.65 V for MWCNTs-COOH/SPE (Fig. 6, curve b), which was attributed to guanine/xanthine (Zhu et al., 2018b; Wu et al., 2011). No reduction peak was obtained during the reverse scan, suggesting an irreversible electron-transfer process. The peak current reached 7.8 μA for MWCNTs-COOH/RhB/SPE (Fig. 6, curve c). In the case of MWCNTs-COOH/AuNPs/SPE, a well-defined anodic peak with a peak current of 8.1 μA appeared (Fig. 6, curve d). The largest peak current (10.9 μA) was obtained at +0.67 V for MWCNTs-COOH/RhB/AuNPs/SPE (Fig. 6, curve e). Its linear detection ranges for CIK cells were 2.5×10^3 to

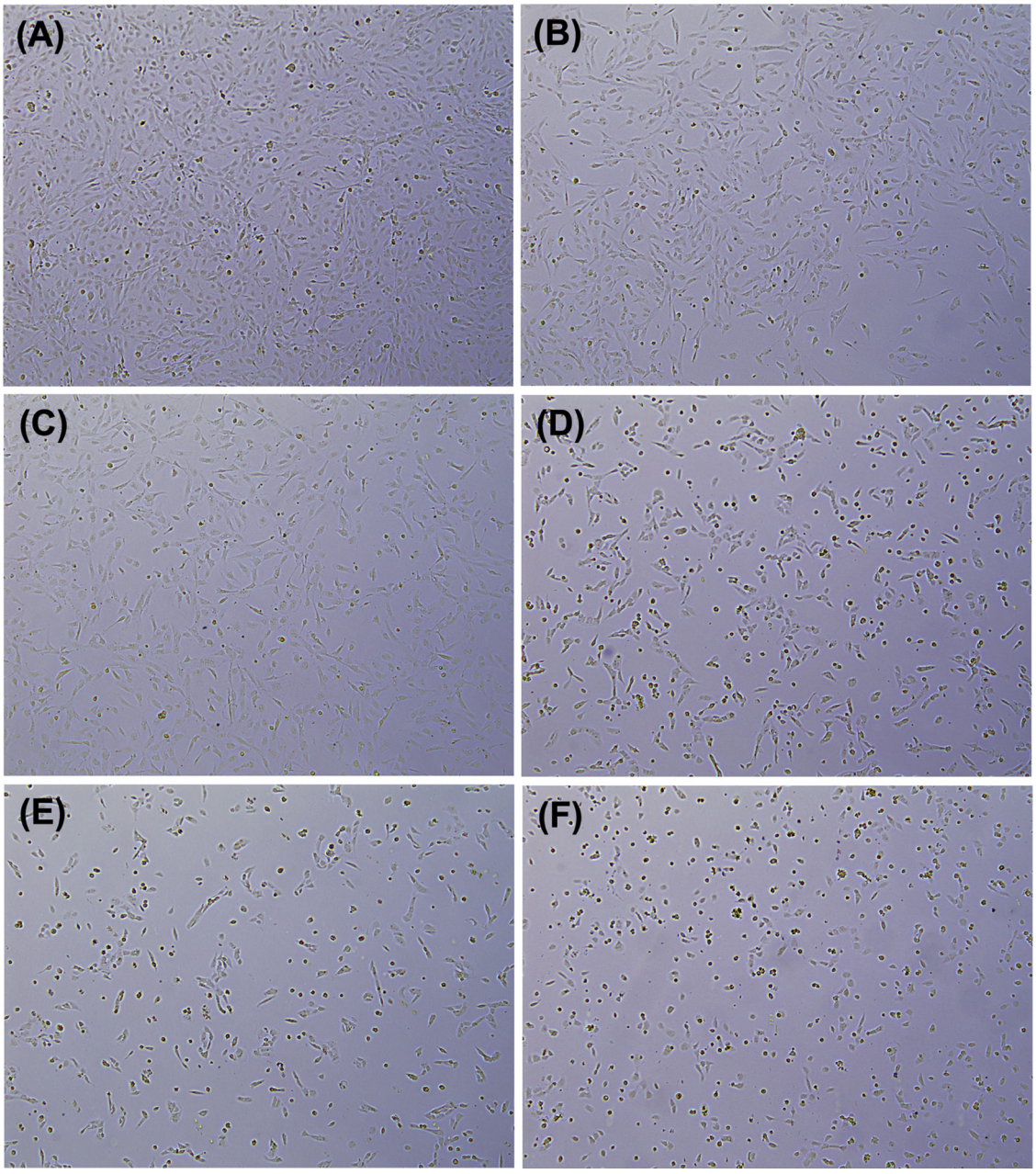

Fig. 8. Morphologies of CIK cells before (A) and after treatment with 230.0 μM BPS (B), BPF (C), BPA (D), BPB (E), and BPAF (F) for 48 h.

6.0×10^6 cells mL^{-1}. The aforementioned results indicated that the MWCNTs-COOH/RhB/AuNPs film had an excellent catalytic performance for the oxidation of intracellular electrochemical substances, which might be attributed to the following aspects. First, MWCNTs-COOH can be used as a wire to promote charge transfer during the electrochemical reaction (Le et al., 2017). The hybrid can prevent the AuNPs from re-stacking, and it has a larger surface area, which helps to enhance the oxidation rate. Second, the synergistic effect among MWCNTs-COOH, RhB, and AuNPs is beneficial to accelerate the electron transfer. Third, the π-π bonds and functional groups contributed to the binding of intracellular electroactive substances onto the electrode surface. The peak current decreased obviously from the second cycle due to the blocking effect of the oxidation product (inset figure in Fig. 6). Therefore, the first cycle was chosen to study the electrochemical behavior of the CIK cells.

3.3. Optimization of accumulate time for the electrochemical determination

The influence of the accumulation time on the peak current of CIK cells was investigated (Fig. S1). The peak current continuously increased during the accumulation time from 0 to 360 s, suggesting that the CIK cells on MWCNTs-COOH/RhB/AuNPs/SPE reached saturation gradually. Thus, 360 s was chosen as the optimal accumulation time.

3.4. Cytotoxicity evaluation of bisphenols on CIK cells

The effects of BPA, BPB, BPF, BPF, and BPAF at various concentrations on CIK cells was studied (Fig. 7). At low concentrations, the bisphenols appeared to stimulate the growth of CIK cells, due to their estrogenic activities. However, all the bisphenols showed significant cytotoxicity in a concentration-dependent manner at higher concentrations. The cytotoxicity was linear to the logarithmic concentration of the bisphenols (insets of Fig. 7). The linear regression equations and correlation coefficients (r) were determined (Table 1). The IC_{50} at 48 h was 21.33, 72.44, 112.20, 158.49, and 173.78 for BPAF, BPB, BPA, BPF, and BPS, respectively. The cytotoxicity ranking order was BPAF > BPB > BPA > BPF > BPS. BPAF and BPB exhibited higher toxicity, whereas BPF and BPS exhibited lower toxicity. The difference in cytotoxicity of the five bisphenols might be attributed to the different substitution patterns on the skeleton structure. BPAF with large hydrophobic radicals (-CF_3) showed the highest toxicity with the lowest IC_{50}, which was consistent with previous findings (Moreman et al., 2017). BPAF was more toxic than BPA to aquatic organisms Danio rerio and Daphnia magna, as well as Zebrafish. The difference in cytotoxicity of bisphenols on CIK cells might be related to metabolic mechanisms. Specifically, BPAF tends to bind to estrogen receptors (ER) more strongly, and could cause adverse reproductive and developmental effects in several different organisms (Ullah et al., 2018; Russo et al., 2018). BPAF exhibited neurotoxicity by disrupting microglial activation and inducing cell death. Therefore, the oxidation peak current related to the nucleotide metabolism declined faster due to the decrease in cell viability. Recent studies have found that BPAF has a slower microbial degradation and a higher adsorption affinity compared with other bisphenols (Choi and Lee, 2017). Therefore, the increasing input of BPAF may result in increased environmental risks, that is, if it continues to replace BPA.

Meanwhile, changes in cell morphology before and after bisphenol treatment for 48 h were investigated (Fig. 8). In the control group (Fig. 8 A), the cell morphology showed a fusiform shape in high-density cells. After treatment with bisphenols, the morphology of CIK cells changed. The cells became round-like and shrank in size and underwent abscission. The number of cells was reduced. The most obvious example of this phenomenon was in BPAF-treated group (Fig. 8 F), indicating that this bisphenol exhibited the strongest toxic effects.

Moreover, considering that organisms are usually exposed to multiple bisphenols rather than a single bisphenol, the combined effects of BPA and its analogues were determined using the sum TU method (Table 2). An additive effect was observed for the binary mixtures of BPAF/BPA and BPB/BPA. Potential synergistic effects were found for the binary mixtures of BPS/BPA and BPF/BPA. However, the toxic site and mode of action of the mixed contaminants are complex and related to their concentrations (Broderius et al., 2010). Therefore, the investigation of the combined toxicity of the binary bisphenols in this study was preliminary, and further research is needed to better understand the interactions and toxicities of bisphenols, especially at environmentally-relevant concentrations.

4. Conclusion

An innovative cell-based biosensor using the sensitive MWCNTs-COOH/RhB/AuNPs composite was developed in this study. The single toxicity and combined toxicities of the binary mixtures of the five bisphenol analogues were evaluated via the changes of the electrochemical signal derived from the nucleotide catabolism of CIK cells. Toxicity data of these bisphenol analogues demonstrated that as compared to BPA, BPAF and BPB are more toxic, implying that the use of these bisphenol analogues to surrogate BPA should be considered carefully. Furthermore, synergistic and additive effects were observed between the binary mixtures of bisphenols. This electrochemical cell-based biosensor could be used for toxicity assessment of dangerous bisphenols. This study provides a miniaturized platform for the toxicity evaluation of bisphenols and enhances our knowledge on the cytotoxicity of BPA alternatives.

Acknowledgments

This work was supported by the National Natural Science Foundation of China (51809044), Environmental Protection Project of Ecology and Environment Department of Jilin Province (2018-10), the Fundamental Research Funds for the Central Universities (2412018QD020), the Jilin Province Science and Technology Development Projects (20190103136JH), and the China Postdoctoral Science Foundation (2018M630314).

Appendix A. Supplementary data

Supplementary material related to this article can be found, in the online version, at doi:https://doi.org/10.1016/j.jhazmat.2019.120908.

References

Alim, S., Vejayan, J., Yusoff, M.M., Kafi, A.K.M., 2018. Recent uses of carbon nanotubes & gold nanoparticles in electrochemistry with application in biosensing: a review. Biosens. Bioelectron. 121, 125–136.

Bagheri Hashkavayi, A., Bakhsh Raoof, J., Ojani, R., Hamidi Asl, E., 2015. Label-free electrochemical aptasensor for determination of chloramphenicol based on gold nanocubes-modified screen-printed gold electrode. Electroanalysis 27, 1449–1456.

Broderius, S.J., Kahl, M.D., Hoglund, M.D., 1995. Use of joint toxic response to define the primary mode of toxic action for diverse industrial organic chemicals. Environ. Toxicol. Chem. 14, 1591–1605.

Broderius, S.J., Kahl, M.D., Elonen, G.E., Hammermeister, D.E., Hoglund, M.D., 2010. A comparison of the lethal and sublethal toxicity of organic chemical mixtures to the fathead minnow (pimephales promelas). Environ. Toxicol. Chem. 24, 3117–3127.

Charoenkitamorn, K., Chaiyo, S., Chailapakul, O., Siangproh, W., 2018. Low-cost and disposable sensors for the simultaneous determination of coenzyme Q10 and α-lipoic acid using manganese (IV) oxide-modified screen-printed graphene electrodes. Anal. Chim. Acta 1004, 22–31.

Choi, Y.J., Lee, L.S., 2017. Aerobic soil biodegradation of bisphenol (BPA) alternatives bisphenol S and bisphenol AF compared to BPA. Environ. Sci. Technol. 51, 13698–13704.

Dinh, N.X., Quy, N.V., Huy, T.Q., Le, A.T., 2015. Decoration of silver nanoparticles on multiwalled carbon nanotubes: antibacterial mechanism and ultrastructural analysis. J. Nanomater. 16, 63.

Guo, X., Wang, Q., Li, J., Cui, J., Zhou, S., Hao, S., Wu, D., 2015. A mini-electrochemical system integrated micropipet tip and pencil graphite electrode for detection of anticancer drug sensitivity in vitro. Biosens. Bioelectron. 64, 594–596.

Guo, C.X., Lei, Y., Li, C.M., 2011. Porphyrin functionalized graphene for sensitive electrochemical detection of ultratrace explosives. Electroanalysis 23, 885–893.

Hassani, S., Akmal, M.R., Salek-Maghsoudi, A., Rahmani, S., Ganjali, M.R., Norouzi, P., Abdollahi, M., 2018. Novel label-free electrochemical aptasensor for determination of Diazinon using gold nanoparticles-modified screen-printed gold electrode. Biosens. Bioelectron. 120, 122–128.
Hou, G., Zhang, R., Hao, X., Liu, C., 2017. An exploration of the effect and interaction mechanism of bisphenol A on waste sludge hydrolysis with multi-spectra, isothermal titration microcalorimetry and molecule docking. J. Hazard. Mater. 333, 32–41.
Jin, H., Zhu, L., 2016. Occurrence and partitioning of bisphenol analogues in water and sediment from Liaohe River Basin and Taihu Lake, China. Water Res. 103, 343–351.
Jirasirichote, A., Punrat, E., Suea-Ngam, A., Chailapakul, O., Chuanuwatanakul, S., 2017. Voltammetric detection of carbofuran determination using screen-printed carbon electrodes modified with gold nanoparticles and graphene oxide. Talanta 175, 331–337.
Johari-Ahar, M., Karami, P., Ghanei, M., Afkhami, A., Bagheri, H., 2018. Development of a molecularly imprinted polymer tailored on disposable screen-printed electrodes for dual detection of EGFR and VEGF using nano-liposomal amplification strategy. Biosens. Bioelectron. 107, 26–33.
Kitamura, S., Suzuki, T., Sanoh, S., Kohta, R., Jinno, N., Sugihara, K., Yoshihara, S., Fujimoto, N., Watanabe, H., Ohta, S., 2005. Comparative study of the endocrine-disrupting activity of bisphenol A and 19 related compounds. Toxicol. Sci. 84, 249–259.
Kwak, J.I., Moon, J., Kim, D., Cui, R., An, Y.J., 2018. Determination of the soil hazardous concentrations of bisphenol A using the species sensitivity approach. J. Hazard. Mater. 344, 390–397.
Le, T.X.H., Flaud, V., Bechelany, M., Cretin, M., Tingry, S., 2017. Optimal direct electron transfer between MWCNTs@COOH/BOD/chitosan layer and porous carbon felt for dioxygen reduction. Electrochim. Acta 230, 373–381.
Li, M., Li, Y.T., Li, D.W., Long, Y.T., 2012. Recent developments and applications of screen-printed electrodes in environmental assays–A review. Anal. Chim. Acta 734, 31–44.
Li, T., Liu, Z., Wang, L., Guo, Y., 2016. Gold nanoparticles/Orange II functionalized graphene nanohybrid based electrochemical aptasensor for label-free determination of insulin. RSC Adv. 6, 30732–30738.
Liao, C., Kannan, K., 2014. A survey of bisphenol A and other bisphenol analogues in foodstuffs from nine cities in China. Food Addit. Contam. 31, 319–329.
Lin, Y., Liu, K., Liu, C., Yin, L., Kang, Q., Li, L., Li, B., 2014. Electrochemical sensing of bisphenol A based on polyglutamic acid/amino-functionalised carbon nanotubes nanocomposite. Electrochim. Acta 133, 492–500.
Liu, Y., Zhang, S., Song, N., Guo, R., Chen, M., Mai, D., Yan, Z., Han, Z., Chen, J., 2017. Occurrence, distribution and sources of bisphenol analogues in a shallow Chinese freshwater lake (Taihu Lake): implications for ecological and human health risk. Sci. Total Environ. 599, 1090–1098.
Magar, H.S., Ghica, M.E., Abbas, M.N., Brett, C.M., 2017. A novel sensitive amperometric choline biosensor based on multiwalled carbon nanotubes and gold nanoparticles. Talanta 167, 462–469.
Moreman, J., Lee, O., Trznadel, M., David, A., Kudoh, T., Tyler, C.R., 2017. Acute toxicity, teratogenic, and estrogenic effects of bisphenol A and its alternative replacements bisphenol S, bisphenol F, and bisphenol AF in zebrafish embryo-larvae. Environ. Sci. Technol. 51, 12796–12805.
Mu, X., Huang, Y., Li, X., Lei, Y., Teng, M., Li, X., Wang, C., Li, Y., 2018. Developmental effects and estrogenicity of bisphenol A alternatives in a zebrafish embryo model. Environ. Sci. Technol. 52, 3222–3231.
Ochiai, L.M., Agustini, D., Figueiredo-Filho, L.C., Banks, C.E., Marcolino-Junior, L.H., Bergamini, M.F., 2017. Electroanalytical thread-device for estriol determination using screen-printed carbon electrodes modified with carbon nanotubes. Sensor. Actuat. B-Chem. 241, 978–984.
Qiu, W., Yang, M., Liu, S., Lei, P., Hu, L., Chen, B., Wu, M., Wang, K.J., 2018. Toxic effects of bisphenol S showing immunomodulation in fish macrophages. Environ. Sci. Technol. 52, 831–838.
Russo, G., Capuozzo, A., Barbato, F., Irace, C., Santamaria, R., Grumetto, L., 2018. Cytotoxicity of seven bisphenol analogues compared to bisphenol A and relationships with membrane affinity data. Chemosphere 201, 432–440.
Salgado-Figueroa, P., Gutierrez, C., Squella, J.A., 2015. Carbon nanofiber screen printed electrode joined to a flow injection system for nimodipine sensing. Sensor. Actuat. B-Chem. 220, 456–462.
Saxena, U., Goswami, P., 2012. Electrical and optical properties of gold nanoparticles: applications in gold nanoparticles-cholesterol oxidase integrated systems for cholesterol sensing. J. Nanopart. Res. 14, 813.
Subramanian, A.S., Tey, J.N., Zhang, L., Ng, B.H., Roy, S., Wei, J., 2016. Synergistic bond strengthening in epoxy adhesives using polydopamine/MWCNT hybrids. Polymer 82, 285–294.
Tan, F., Wang, M., Wang, W., Lu, Y., 2008. Comparative evaluation of the cytotoxicity sensitivity of six fish cell lines to four heavy metals in vitro. Toxicol. In Vitro 22, 164–170.
Tan, S., Li, H., Jin, Y., Yu, H., 2014. In vitro and in vivo effects of sublethal cadmium on the expression of MT2 and ABCC2 genes in grass carp (Ctenopharyngodon idellus). Ecotoxicol. Environ. Safe. 108, 258–264.
Thomas, T., Mascarenhas, R.J., Swamy, B.K., 2012. Poly (Rhodamine B) modified carbon paste electrode for the selective detection of dopamine. J. Mol. Liq. 174, 70–75.
U.S. Food, Drug Administration, 2013. Amended the regulation 21 CFR175 as regards no longer use Bisphenol A in the coating of packaging for powdered and liquid infant formula. Fed. Reg 78 (July (134)), 41840.
Ullah, A., Pirzada, M., Jahan, S., Ullah, H., Shaheen, G., Rehman, H., Siddiqui, M.F., Butt, M.A., 2018. Bisphenol A and its analogs bisphenol B, bisphenol F, and bisphenol S: comparative in vitro and in vivo studies on the sperms and testicular tissues of rats. Chemosphere 209, 508–516.
Villeneuve, D.L., Garcia-Reyero, N., Escalon, B.L., Jensen, K.M., Cavallin, J.E., Makynen, E.A., Durhan, E.J., Kahl, M.D., Thomas, L.M., Perkins, E.J., Ankley, G.T., 2011. Ecotoxicogenomics to support ecological risk assessment: a case study with bisphenol A in fish. Environ. Sci. Technol. 46, 51–59.
Wang, J., 2005. Carbon-nanotube based electrochemical biosensors: a review. Electroanalysis 17, 7–14.
Wang, Y.C., Cokeliler, D., Gunasekaran, S., 2015. Reduced graphene oxide/carbon nanotube/gold nanoparticles nanocomposite functionalized screen-printed electrode for sensitive electrochemical detection of endocrine disruptor bisphenol A. Electroanalysis 27, 2527–2536.
Wu, D.M., Fu, G.L., Wang, J.T., Ge, L.Y., Zhu, J.H., Yuan, X., Liu, J.G., 2011. Voltammetric behavior of the heat-treating PC-3 cells and its application in drug sensitivity test. Electrochem. commun. 13, 623–626.
Yamazaki, E., Yamashita, N., Taniyasu, S., Lam, J., Lam, P.K., Moon, H.B., Jeong, Y., Kannan, P., Achyuthan, H., Munuswamy, N., Kannan, K., 2015. Bisphenol A and other bisphenol analogues including BPS and BPF in surface water samples from Japan, China, Korea and India. Ecotox. Environ. Safe. 122, 565–572.
Yue, X., Song, W., Zhu, W., Wang, J., Wang, Y., 2015. In situ surface electrochemical co-reduction route towards controllable construction of AuNPs/ERGO electrochemical sensing platform for simultaneous determination of BHA and TBHQ. Electrochim. Acta 182, 847–855.
Zanganeh, N., Rajabi, A., Torabi, M., Allahkarami, M., Moghaddas, A., Sadrnezhaad, S.K., 2014. Growth and microstructural investigation of multiwall carbon nanotubes fabricated using electrodeposited nickel nanodeposits and chemical vapor deposition method. J. Mol. Struct. 1074, 250–254.
Zhu, X., Zhang, K., Wang, C., Guan, J., Yuan, X., Li, B., 2016. Quantitative determination and toxicity evaluation of 2, 4-dichlorophenol using poly (eosin Y)/hydroxylated multi-walled carbon nanotubes modified electrode. Sci. Rep. 6, 38657.
Zhu, X., Qin, H., Liu, J., Zhang, Z., Lu, Y., Yuan, X., Wu, D., 2014. A novel electrochemical method to evaluate the cytotoxicity of heavy metals. J. Hazard. Mater. 271, 210–219.
Zhu, X., Wu, G., Lu, N., Yuan, X., Li, B., 2017. A miniaturized electrochemical toxicity biosensor based on graphene oxide quantum dots/carboxylated carbon nanotubes for assessment of priority pollutants. J. Hazard. Mater. 324, 272–280.
Zhu, M., Chen, X.Y., Li, Y.Y., Yin, N.Y., Faiola, F., Qin, Z.F., Wei, W.J., 2018a. Bisphenol F disrupts thyroid hormone signaling and postembryonic development in Xenopus laevis. Environ. Sci. Technol. 52, 1602–1611.
Zhu, X., Zhang, K., Lu, N., Yu, Y., Yuan, X., Guan, J., 2018b. A label-free electrochemical system for comprehensive monitoring of o-chlorophenol. Chemosphere 196, 514–521.
Zhu, X., Zhang, K., Wang, D., Zhang, D., Yuan, X., Qu, J., 2018c. Electrochemical sensor based on hydroxylated carbon nanotubes/platinum nanoparticles/rhodamine B composite for simultaneous determination of 2, 4, 6-trichlorophenol and 4-chlorophenol. J. Electroanal. Chem. Lausanne (Lausanne) 810, 199–206.